Structural and functional insights into *Archaeoglobus fulgidus* m^2G_10 tRNA methyltransferase Trm11 and its Trm112 activator

Can Wang, Nhan Van tran, Vincent Jactel, Vincent Guérineau, Marc Graille

11068–11082 *Nucleic Acids Research, 2020, Vol. 48, No. 19* *Published online 9 October 2020*
doi: 10.1093/nar/gkaa830

Structural and functional insights into *Archaeoglobus fulgidus* m^2G_{10} tRNA methyltransferase Trm11 and its Trm112 activator

Can Wang[1], Nhan van Tran[1], Vincent Jactel[2], Vincent Guérineau[3] and Marc Graille[1,*]

[1]Laboratoire de Biologie Structurale de la Cellule (BIOC), CNRS, Ecole polytechnique, Institut Polytechnique de Paris, F-91128 Palaiseau, France, [2]Laboratoire de Synthèse Organique (LSO), CNRS, Ecole polytechnique, ENSTA, Institut Polytechnique de Paris, F-91128 Palaiseau, France and [3]Université Paris-Saclay, CNRS, Institut de Chimie des Substances Naturelles, UPR 2301, 91198, Gif-sur-Yvette, France

Received August 04, 2020; Revised September 11, 2020; Editorial Decision September 15, 2020; Accepted September 17, 2020

ABSTRACT

tRNAs play a central role during the translation process and are heavily post-transcriptionally modified to ensure optimal and faithful mRNA decoding. These epitranscriptomics marks are added by largely conserved proteins and defects in the function of some of these enzymes are responsible for neurodevelopmental disorders and cancers. Here, we focus on the Trm11 enzyme, which forms N^2-methylguanosine (m^2G) at position 10 of several tRNAs in both archaea and eukaryotes. While eukaryotic Trm11 enzyme is only active as a complex with Trm112, an allosteric activator of methyltransferases modifying factors (RNAs and proteins) involved in mRNA translation, former studies have shown that some archaeal Trm11 proteins are active on their own. As these studies were performed on Trm11 enzymes originating from archaeal organisms lacking TRM112 gene, we have characterized Trm11 (*Af*Trm11) from the *Archaeoglobus fulgidus* archaeon, which genome encodes for a Trm112 protein (*Af*Trm112). We show that *Af*Trm11 interacts directly with *Af*Trm112 similarly to eukaryotic enzymes and that although *Af*Trm11 is active as a single protein, its enzymatic activity is strongly enhanced by *Af*Trm112. We finally describe the first crystal structures of the *Af*Trm11-Trm112 complex and of Trm11, alone or bound to the methyltransferase inhibitor sinefungin.

INTRODUCTION

Transfer RNAs (tRNAs) are adaptor molecules involved in the translation process of the DNA sequence of a gene into the protein it encodes. They decode the mRNA codon present in the ribosomal A-site and bring the corresponding amino acid into the ribosomal peptidyl transferase center during protein synthesis. Thus, tRNAs directly participate to the accuracy and fidelity of mRNA translation but it is increasingly evident that they also contribute to correct folding of nascent polypeptides by tuning translational speed (1–3). These roles are achieved thanks to the presence of tens of various chemical modifications decorating tRNAs either on bases or on riboses (4,5). Some of those modifications are known to stabilize the tRNA structure, to participate in tRNA binding to the ribosomal A-site or to be important for tRNA recognition by cognate aminoacyl tRNA synthetases (4,6,7). Others are present in the tRNA anticodon stem loop and are important for decoding, allowing for instance a single tRNA to recognize several codons (5,8). Although many of the enzymes catalyzing these tRNA modifications are conserved throughout evolution between either two or three domains of life, the importance of these modifications for many organisms emerged only recently. Indeed, growing studies highlight the influence of these tRNA modifications in cell development, protein homeostasis and physiopathologies such as diabetes, cancers and neurological disorders (9–12).

In eukaryotes, several tRNA modifications are written by multi-protein complexes (13). This is indeed the case of the KEOPS complex responsible for the deposition of t^6A (N^6-threonylcarbamoyladenosine) at position 37 of tRNAs decoding ANN codons (14) and of the Elongator complex (formed by the Elp1–6 proteins), which catalyzes the formation of cm^5U (5-carboxymethyluridine) at the wobble position of several tRNAs (15). Interestingly, the human TRMT112 protein (Trm112 in yeast) acts as an allosteric regulator of several *S*-adenosyl-L-methionine (SAM) dependent MTases, which modify tRNAs, rRNAs or protein factors directly contributing to the protein synthesis process (16). As complexes with WBSCR22 (Bud23 in yeast) and METTL5 (no orthologue exists in *Saccharomyces cerevisiae* yeast), TRMT112 contributes to the biogenesis of

*To whom correspondence should be addressed. Tel : +33 1 69 33 48 90; Email: marc.graille@polytechnique.edu

the 40S ribosomal subunit by respectively catalyzing the formation of N^7-methylguanosine (m^7G_{1636} in human and m^7G_{1575} in yeast) and N^6-methyladenosine (m^6A_{1832} in human) on 18S rRNA (17–21). The TRMT112-HEMK2 complex (Trm112-Mtq2 in yeast) modifies the glutamine side chain of the universally conserved GGQ motif (for Gly-Gly-Gln) found in class I eRF1 release factors, which enters into the peptidyl transferase center to catalyze the release of newly synthesized proteins from ribosomes (22,23). TRMT112 also contributes to translation elongation by interacting with and activating two tRNA MTases: ALKBH8 and TRMT11 (respectively, Trm9 and Trm11 in *S. cerevisiae*). The TRMT112–ALKBH8 complex catalyzes the formation of mcm^5U (5-methoxycarbonylmethyluridine) from cm^5U, itself formed by the Elongator complex, at position 34 of some tRNAs (24–27). In humans and other metazoa, the TRMT112-ALKBH8 complex further hydroxylates mcm^5U to form (S)-$mchm^5U$ (5-methoxycarbonylhydroxymethyluridine; (28,29)). The yeast Trm11–Trm112 complex (and most probably the human TRMT11–TRM112 complex, although this has not yet been experimentally determined) methylates some tRNAs at position G_{10} of the aminoacyl acceptor stem loop to generate m^2G_{10} (N^2-methylguanosine; (30,31)). Finally, TRMT112 interacts with TRMT9B, a second orthologue of Trm9, whose substrate and biochemical function have not yet been identified (32). Altogether, while *S. cerevisiae* Trm112 interacts with 4 MTases, human TRMT112 interacts with at least six MTases. Structural studies of Trm112-MTase complexes (only the Trm11–Trm112 complex has been resistant to X-ray crystallography studies so far) have shown that all these MTases compete to interact in a very similar way with Trm112 (18,20,23,27,31). Cell biology and biochemical approaches have further revealed that in the case of many of these MTases, their interaction with Trm112 is mandatory for their cellular stability and their ability to interact with SAM, but also contributes to substrate binding (19,20,23,31,33–35).

Recently, we have shown that the Trm112 orthologue (*Hvo*Trm112) from *Haloferax volcanii*, the archaeal model organism, interacts with an even larger number of MTases, including orthologues of eukaryotic HEMK2/Mtq2, METTL5, ALKBH8/Trm9 and probably TRMT11/Trm11 (20,36). The presence of a protein annotated as Trm11 (also known as $TrmG_{10}$ in archaea) among the most enriched putative partners of *Hvo*Trm112 was rather unexpected considering former studies conducted on some archaeal Trm11 (37,38). Indeed, the enzymatic activities of Trm11 from *P. abyssii* and *Thermococcus kodakarensis* archaea have been characterized, revealing that in these organisms, Trm11 is active on its own and is able to catalyze formation of m^2G_{10} but also of $N^{2,2}$-dimethylguanosine ($m^2{}_2G_{10}$; (37–39)) on different tRNAs. Such modifications have also been identified at this position in *H. volcanii* archaeal tRNAs (40). Trm11 proteins are composed of two essential domains (37,38,41): an N-terminal THUMP domain, which has been shown to interact with the aminoacyl acceptor arm of the tRNAs (42), fused to a C-terminal MTase domain. Trm11 proteins are ubiquitously found in eukaryotes and archaea but not bacteria, strongly arguing in favor of an important physiological role in these two domains of life, where most factors participating in mRNA translation are very similar (43). This was recently confirmed in *T. kodakarensis* where the TRM11 gene and hence m^2G_{10} and $m^2{}_2G_{10}$ tRNA modifications, proved very important for growth at high temperature (93–95°C; (44,45)), probably due to the contribution of these modifications to correct tRNA folding.

Our former bioinformatics analysis revealed that Trm112 archaeal orthologues are absent in Thermococcales (to which *T. kodakarensis* and *P. abyssi* belong) and Methanobacteriales, rationalizing that Trm11 proteins from these organisms are active on their own (16). The presence of putative Trm11 within the list of proteins co-purifying with Trm112 in *H. volcanii* (36) led us to investigate whether in archaea possessing Trm112 proteins, this latter interacts with and activates Trm11-like proteins as previously shown for budding yeast proteins (31). Here, we structurally and functionally characterize a gene product from the *Archaeoglobus fulgidus* archaeon as a tRNA methyltransferase and demonstrate that it interacts directly with Trm112 protein (hereafter named *Af*Trm112). We further show that *Af*Trm112 enhances its enzymatic activity.

MATERIALS AND METHODS

Heterologous expression and purification of *A. fulgidus* proteins

A DNA sequence optimized for heterologous co-expression in *E. coli* was designed to produce *A. fulgidus* AF_RS01245 (*Af*Trm112) and AF_1257 (with a C-terminal His_6-tag) gene products. This fragment was obtained by *de novo* synthesis (Integrated DNA Technologies, Belgium) and cloned into pET21-a between *Nde*I and *Xho*I sites to yield plasmid pMG836. To express the AF_1257 protein alone, a DNA fragment encoding a C-terminally His-tagged version of AF_1257 was inserted into a *BamH*I/*Xho*I-digested vector pET21a to generate plasmid pMG964. A second plasmid (pMG979) expressing AF_1257 was obtained by inserting the polymerase chain reaction (PCR) product generated using primers oMG682/oMG683 and pMG836 as template, into pET21a between *Nde*I and *Xho*I sites. Oligonucleotides oMG676/oMG677 were used to generate the pMG989 plasmid encoding for the AF_1257-D248A mutant and the *Af*Trm112 proteins by site directed mutagenesis using pMG836 as template (46). Details on plasmids and oligonucleotides are listed in Supplementary Table S1.

The *Af*Trm112 and AF_1257 proteins were co-expressed in *E. coli* BL21 (DE3) Gold (Agilent technologies) using plasmid pMG836. Large-scale expression was done in 1 L of auto-inducible terrific broth media (ForMedium AIMTB0260) supplemented with ampicillin (100 μg/ml), first at 37°C for 3 h and then at 18°C overnight. The cells were harvested by centrifugation at 4000 rpm for 30 min and the pellets were resuspended in 30 ml of lysis buffer (0.3 M NaCl, 50 mM Tris-HCl pH 7.5, 5 mM β-mercaptoethanol, 10 μM $ZnCl_2$ and 10 mM Imidazole). The cells were lysed by sonication on ice and the lysate clearance was performed by centrifugation at 20 000 g for 45 min. The supernatant was incubated with 16 μg of Benzonase at 4°C for 20 min and then heated at 62°C for 30 min. Precipitated proteins

were removed by centrifugation at 20 000 g for 30 min. The supernatant was applied on Ni-NTA resin pre-equilibrated with the lysis buffer, incubated at 4°C on a rotating wheel for 1 h, followed by a washing step with 30 ml of washing buffer (2 M NaCl, 50 mM Tris–HCl pH 7.5, 5 mM β-mercaptoethanol, 10 μM $ZnCl_2$ and 20 mM imidazole). The AF_1257-*Af*Trm112 complex was eluted by 15 ml of elution buffer (0.3 M NaCl, 50 mM Tris–HCl pH7.5, 5 mM β-mercaptoethanol, 10 μM $ZnCl_2$ and 350 mM Imidazole), followed by concentrating up to 1 ml by a 10 kDa cutoff concentrator. The protein sample was then diluted to 5 mL using buffer A (50 mM NaCl, 20 mM Tris–HCl pH 7.5, 5 mM β-mercaptoethanol, 10 μM $ZnCl_2$) and injected on an ion-exchange chromatography Mono Q column. The protein complex was eluted by a NaCl linear gradient from 50 mM (buffer A) to 1 M (buffer B: 1 M NaCl, 20 mM Tris–HCl pH 7.5, 5 mM β-mercaptoethanol, 10 μM $ZnCl_2$). The fractions containing AF_1257-*Af*Trm112 were collected and concentrated up to 5 ml, followed by injection on a S75-16/60 size-exclusion column (GE Healthcare) with buffer B. The fractions containing the protein complex were collected and concentrated to 20 mg/ml.

The wild-type and D248A mutant AF_1257 proteins were expressed as described above using plasmids pMG979 and pMG989. The purification protocol for these two proteins was similar to that of AF_1257-*Af*Trm112 except that the ion exchange chromatography purification step was omitted.

Size exclusion chromatography-multi-angle laser light scattering (SEC-MALLS)

The samples (100 μl at 1 mg/ml) were injected at a flow rate of 0.75 ml/min on a Superdex™ 200 Increase 10/300 GL column (GE-Healthcare) using buffer B. Elution was followed by a UV–visible spectrophotometer, a RID-20A refractive index detector (Shimadzu), a MiniDawn TREOS detector (Wyatt Technology). The data were collected and processed with the program ASTRA 6.1 (Wyatt Technology). M_w was directly calculated from the absolute light scattering measurements using a dn/dc value of 0.183.

In vitro tRNA methylation assay

The plasmid used to express *E. coli* methionyl-tRNA ($tRNA_i^{Met}$) in *E. coli* XL1-blue is a kind gift from Dr Y. Mechulam (Ecole polytechnique, France) (47). This tRNA was expressed and purified as previously described (48). The enzymatic assays were performed by mixing 75 pmol of *E. coli* $tRNA_i^{Met}$ with 3 pmol of enzyme (AF_1257 ± *Af*Trm112) and 2 μM of SAM (comprising 0.2 μM of [^{3}H]-SAM, Perkin Elmer) in MTase buffer (25 mM K-phosphate pH 7.5, 50 μM EDTA, 5 mM $MgCl_2$, 5 mM NH_4Cl) with total volume of 50 μl. The reaction was incubated at 65°C for 2 h and stopped by adding 5 mL of cold trichloroacetic acid (TCA 5%) containing 0.5% of methionine, then 20 μl of RNA carrier 4 mg/ml, Colnbrook-Bucks-England), and followed by filtration on glass microfiber filters (Whatman GF/C). Beckman Coulter LS6500 scintillation counter was used to determine [^{3}H] incorporation. The initial velocities (Vi) for each tRNA concentration were calculated using the equation: $C_{tRNA} = V_i{*}(1 - \exp(-nt))/n$ where C_{tRNA} is the concentration of methylated tRNA, t the time in minutes, V_i the initial enzyme cycling velocity, and n the relaxation rate constant of V_i by fitting the experimental spots with the ORIGIN® software according to Cao *et al.* (49). Initial velocities were plotted as a function of the tRNA concentration and the data were fitted to the Michaelis–Menten equation using the ORIGIN software. The K_m, k_{cat} and k_{cat}/K_m values were calculated from these curve fitting. All reactions were performed in triplicates.

HPLC-MS for determination of tRNA modification

The $tRNA_i^{Met}$ (20 μg corresponding to 834 pmol) was incubated overnight either alone or with 33 pmol of either AF_1257 or AF_1257-*Af*Trm112 in MTase buffer (25 mM K-phosphate pH 7.5, 50 μM EDTA, 5 mM $MgCl_2$, 5 mM NH_4Cl) supplemented with SAM (556 pmol) at 65°C. Two volumes of 100% cold ethanol were added into the reaction system for tRNA precipitation, followed by centrifugation to discard the supernatant. The pellet was then resuspended by 20 μl of 10 mM Tris–HCl pH 7.5. For digestion, 20 μg of *in vitro* modified $tRNA_i^{Met}$ were firstly denatured by heating at 95°C for 5 min and then quickly transferred into ice for 5 min. Next, tRNAs were incubated with 4 U of nuclease P1 (SIGMA: #N8630–1VL) and 4.4 μl of 100 mM ammonium acetate pH 5.3 at 42°C for 2 h. 0.02 U of phosphodiesterase (SIGMA: #P3243-1VL) and 4 μl of 1 M ammonium bicarbonate were then added and the reaction was incubated at 37°C for 1 h. Finally, 2 U of alcaline phosphatase (SIGMA: #P4252-100UN) were added prior to incubation at 37°C for 1 h. The digested tRNAs were transferred to rinsed Microcon concentrators (MCWO YM-10) and centrifuged at 16 000 g at 4°C for at least 10 min. The filtrates were stored at –20°C for further analysis. These reactions were performed in triplicates.

Nucleosides were analyzed by HPLC–MS using an Agilent Technologies 1260 Infinity liquid chromatography (LC) coupled to an Agilent Technologies 6100 Series G6120B electrospray mass spectrometer. Nucleotides were separated on a C_{18} column (Hypersil GOLD aQ, Thermo Scientific, 3 μm, 150 mm × 2.1 mm) at 36°C and a 0.4 ml/min flow rate as described in (50). Before each run, the column was equilibrated for 30 min with 100% of 0.1% aqueous formic acid. The elution from the HPLC column was continuously analyzed by electrospray ionisation (ESI) mass spectrometry (gaz temperature of 350°C, gas flow of 12 l/min, nebulizer gas of 1.5 l/min and capillary voltage of 3000 V). During separation, the ionized adducts of nucleosides were detected by either a positive or negative polarity mode over the m/z range of 100–700. The m^2G and $m^2{}_2G$ nucleoside standards were obtained respectively from SIGMA (#M4004) and Berry & Associates (#PR3702).

MALDI-TOF MS-MS to map modifications on tRNAs

$tRNA_i^{Met}$ (15 μg corresponding to 625 pmol) alone or mixed with equimolar quantities of either AF_1257 or AF_1257-*Af*Trm112 complex were incubated overnight in MTase buffer containing equimolar quantities of SAM at 65°C. Modified tRNAs were separated from the reaction system by precipitation with 2 volumes of 100% cold

ethanol. Prior to digestion, *in vitro* modified $tRNA_i^{Met}$ and RNase A were both washed in 100 mM ammonium acetate solution through several cycles of concentration using Vivaspin 500 (MWCO 500; Sartorius). Next, modified tRNAs (15 μg) were incubated with 10 μg of RNase A at 37°C for 2 h. The samples were then concentrated around 10 μl. One microliter of digest was mixed with 9 μl of 3-hydroxypicolinic acid (3-HPA as the matrix for MALDI-TOF analyses; 40 mg/ml in water:acetonitrile 50:50) and 1 μl of the mixture was spotted on the MALDI plate and air-dried ('dried droplet' method). 3-HPA (Sigma-Aldrich Co) was of the highest grade available and used without further purification. MALDI-TOF MS and MALDI-TOF/TOF MS/MS analyses were performed using an UltrafleXtreme mass spectrometer (Bruker Daltonics, Bremen). Acquisitions were performed in reflector positive ion mode. The laser intensity was set just above the ion generation threshold to obtain peaks with the highest possible signal-to-noise (S/N) ratio without significant peak broadening. For MS/MS experiments, argon was used as collision gas. All data were processed using the program FlexAnalysis (Bruker Daltonics, Bremen). Acquisitions were performed in positive ion mode. These analyses were performed in triplicates.

Crystallization and structure determination

Crystals of the AF_1257-*Af*Trm112 complex were obtained at 24°C by mixing equal volume of protein complex (20 mg/ml) and crystallization condition (1.6 M ammonium sulfate, 0.1M MES pH 6.5; 10% 1,4-dioxane). Prior to data collection, these crystals were transferred into the crystallization solution supplemented first with 15% and then 30% (v/v) ethylene glycerol, followed by flash-freezing in liquid nitrogen. Crystals diffracted up to 3 Å resolution at Synchrotron SOLEIL (Saint-Aubin, France) on beamline Proxima-1A at 100 K. To solve the structure of this complex, we took advantage of the presence of a zinc atom bound to *Af*Trm112 zinc-binding domain and collected three datasets around the zinc anomalous edge for Zn-MAD phasing. These datasets were processed with the XDS program and scaled with XSCALE (51). Due to the presence of two copies of the AF_1257-*Af*Trm112 complex in the asymmetric unit, the locations of two zinc atoms found using the SHELXD program (52) were used to obtain experimental phases with SHARP program (53). Density modification and NCS averaging was further performed using the RESOLVE program (54) to improve the quality of the electron density map. The model for the AF_1257-*Af*Trm112 complex was then built in the experimental electron density maps using COOT (55).

In parallel, we solved the structures of AF_1257-*Af*Trm112 bound to sinefungin (SFG; SIGMA: #S8559), a well-known inhibitor of SAM-dependent MTases and of AF_1257 alone or bound to SFG from crystals obtained from experiments aimed at crystallizing the AF_1257-Trm112-tRNA and AF_1257-tRNA complexes. Those tRNA–protein complexes were reconstituted by mixing equal amount of each component and then purification by size-exclusion chromatography on a S75-16/60 column (GE Healthcare) using a specific buffer (25 mM Tris–HCl pH 7.5, 50 μM EDTA, 5 mM $MgCl_2$, 5 mM NH_4Cl). Co-crystals of AF_1257-Trm112-SFG complex were obtained at 24°C by mixing reconstituted AF_1257-Trm112–*E. coli* $tRNA_i^{Met}$ complex (20 mg/ml) with 10-fold molar excess of SFG and equal volume of crystallization solution (containing 0.1 M sodium citrate pH 6; 9% PEG 4000, 0.1 M ammonium sulfate). Crystals of AF_1257 were obtained by mixing AF_1257–*E. coli* $tRNA_i^{Met}$ complex (20 mg/ml) with 0.1 M sodium citrate pH 6, 18% PEG 4000, 20% isopropanol for the apo-form or with 0.1 M HEPES pH 7, 0.8 M Na/K Tartrate for the SFG-bound form. All crystals were cryo-protected by transfer into crystallization solution supplemented first with 15% and then 30% (v/v) ethylene glycerol, followed by flash freezing in liquid nitrogen. All datasets were collected at synchrotron SOLEIL (Saint-Aubin, France) on beam-line Proxima-2A at 100 K, and processed as described above for the AF_1257-*Af*Trm112 complex. These structures were solved by molecular replacement with the PHASER program (56) and using the structures of AF_1257 and eventually *Af*Trm112 as templates. Several cycles of structure building and refinement were accomplished by COOT and BUSTER (57) programs.

Statistics for datasets processing and structure refinement are summarized in Table 1.

ITC experiments

ITC experiments were performed at 50°C using an ITC-200 microcalorimeter (MicroCal). Proteins and SAM were prepared in buffer B. For all titration experiments, 20 injections of 2 μl of SAM (500 μM) were added to the target (either AF_1257 or AF_1257-*Af*Trm112 at 50 μM) at intervals of 180 s. The heat of dilution of the titrant was determined from the peaks measured after full saturation of the target by the titrant. A theoretical curve assuming a one-binding site model calculated with the ORIGIN® software gave the best fit to the experimental data. This software uses the relationship between the heat generated by each injection and ΔH (enthalpy change), Ka (association binding constant), n (the number of binding site per monomer), the total target concentration, and the free and total titrant concentrations.

Thermal shift assay (TSA)

TSA experiments were performed using a CFX96 real-time PCR machine (BioRad). AF_1257 or AF_1257-*Af*Trm112 (25 μg each) were incubated in different buffers (MTase buffer or 16 mM Tris-HCl pH 7.5, 4 mM β-mercaptoethanol, 8 μM $ZnCl_2$ supplemented with either 0.4 M NaCl or 0.8 M NaCl) in the presence of SYPRO-Orange dye (5×; Invitrogen, #S-6651). After a brief incubation at 20°C (30 sec), the temperature was linearly increased from 20 to 95°C by steps of 0.5°C/s. The Tm values were determined as the inflexion point of the curve depicting the resulting fluorescence intensity as a function of temperature.

RESULTS

Archaeal Trm112 interacts with AF_1257 and enhances its enzymatic activity

In *S. cerevisiae*, Trm11 catalyzes the formation of N^2-monomethylguanosine (m^2G_{10}) in tRNAs but requires the

Table 1. Data collection and refinement statistics

Data collection	***Af*Trm11-Trm112**				***Af*Trm11**	
	Zn-SAD			SFG	apo	SFG
	Peak	Inflexion	Remote			
Space group	$P3_121$			$P2_12_12_1$	$P4_12_12$	$P2_1$
Unit cell parameters (a; b; c; α; β; γ)	184.8 Å; 184.8 Å; 91.4 Å; 90°; 90°; 120°			75.36 Å; 92.94 Å; 91.4 Å; 90°; 90°; 90°	73.18 Å; 73.18 Å; 155.09 Å; 90°; 90°; 90°	41.5 Å; 74.17 Å; 112.89 Å; 90°; 93.5°; 90°
Wavelength (Å)	1.27806	1.28308	0.97857	0.980096	0.980114	0.980114
Resolution (Å)		50–2.9 (2.98–2.9)		50–2.2 (2.33–2.2)	50–2.75 (2.91–2.75)	50–1.9 (2–1.9)
R_{merge} (%)	18.9 (266)	16.7 (227.1)	10.8 (132)	6.5 (123.1)	14.6 (183.6)	11.3 (110.3)
I / σI	11.3 (1.1)	11.3 (1.2)	16.7 (1.8)	13.1 (1.1)	12.2 (1.1)	10.2 (1.2)
Completeness (%)	99.8 (100)	99.9 (100)	100 (100)	99.6 (98.9)	99.7 (98.7)	98.2 (93.2)
$CC_{1/2}$ (%)	99.7 (48.8)	99.7 (46.2)	99.9 (68.1)	99.8 (52.2)	99.8 (46.2)	99.6 (58.5)
Redundancy	10.2	10.3	10.5	4.5	8.6	3.3
Observed reflections	791457	799767	809004	165813	99451	18850
Unique reflections	77254	77342	77371	36999	11597	54554
Refinement						
Resolution (Å)				39.6–2.2	49.1–2.75	21.7–1.9
R/R_{free} (%)				19.8/21.7	19.9/25.5	22.3/25.6
Number of atoms						
Protein/SFG				3037/27	2615	5281/57
Water				64	6	196
Others				59	4	16
B-factors (Å2)						
Protein/SFG				72.3/53.8	80.2	39/29.3
Water				64.7	63.2	41.6
Others				89.3	114.4	58.5
R.m.s deviations						
Bond lengths (Å)				0.010	0.010	0.010
Bond angles (°)				1.15	1.20	1.09
PDB code				6ZXW	6ZXY	6ZXV

assistance of Trm112 (30,31). Unlike yeast Trm11, archaeal $TrmG_{10}$ enzymes from *P. abyssi* and *T. kodakarensis* (hereafter named *Pab*Trm11 and *Tko*Trm11, respectively) add both m^2G_{10} and $N^{2,2}$-dimethylguanosine ($m^2{}_2G_{10}$) modifications to tRNAs and are active on their own (37–39). As no gene encoding for a Trm112 orthologue has been detected in *P. abyssi* or *T. kodakarensis*, we have investigated whether when present in an archaeal organism, the Trm112 protein interacts with Trm11 and influences its enzymatic activity. First evidence for an interaction between these two proteins in archaea came from our former investigation showing that Trm11 is one of the most potent partners of *H. volcanii* Trm112 (36). However, it was not possible to experimentally validate the interaction between these two proteins as *H. volcanii* Trm11 could not be expressed as a soluble protein either alone or upon co-expression with Trm112. We then decided to focus on orthologous proteins from the *A. fulgidus* archaeon. We selected the AF_1257 and AF_RS01245 genes, which encode for proteins sharing 37% and 50% sequence identities with *H. volcanii* Trm11 and Trm112, respectively. These candidate genes are then very likely to encode for *A. fulgidus* Trm11 and Trm112 (hereafter *Af*Trm112) orthologues.

We expressed a His-tagged version of AF_1257 either alone or in the presence of an untagged version of *Af*Trm112 in *E. coli*. Interestingly, in both conditions, AF_1257 was expressed as a soluble protein and was retained on NiNTA resin (Figure 1A). This allowed us to further purify AF_1257 and most interestingly, to detect a specific band migrating around 6.8 kDa and co-purifying with AF_1257 only when *Af*Trm112 was co-expressed with the latter (Figure 1A). The protein corresponding to this band was identified as *Af*Trm112 by mass spectrometry. Besides, AF_1257 alone was not as stable as when in complex with *Af*Trm112. Indeed, it had a strong tendency to precipitation at low salt concentration (50–100 mM) while the complex did not. Furthermore, we determined the melting temperature of AF_1257 alone (from 72.8 to 77.1°C depending on the tested buffer) and of the AF_1257-*Af*Trm112 complex (above 92°C in both conditions) revealing that *Af*Trm112 strongly protects AF_1257 from thermal denaturation (Supplementary Figure S1 and Table S2). SEC-MALLS investigation further confirmed that AF_1257 and *Af*Trm112 form a tight heterodimer of 42.3 kDa in solution (the theoretical molecular weight of this heterodimeric complex is 44.3 kDa) while AF_1257 alone is monomeric in solution (35.8 kDa; Figure 1B). Altogether, these results demonstrate that *Af*Trm112 interacts physically and stably with AF_1257 and stabilizes the latter, similarly to the effect of *S. cerevisiae* Trm112 on Trm11 (31).

In order to investigate the biochemical function of AF_1257 alone or in complex with *Af*Trm112 as tRNA methyltransferase, *E. coli* $tRNA_i^{Met}$ was used as substrate for *in vitro* enzymatic assays. This tRNA, which contains a G at position 10, was over-expressed in *E. coli* and due to the absence of the m^2G_{10} or $m^2{}_2G_{10}$ modifications in bacteria, it should be an appropriate substrate. The enzymatic activity was quantified by measuring the incorporation of radioactivity from [^{3}H]-SAM into tRNAs upon methylation. The AF_1257 protein was able to methylate tRNA by itself

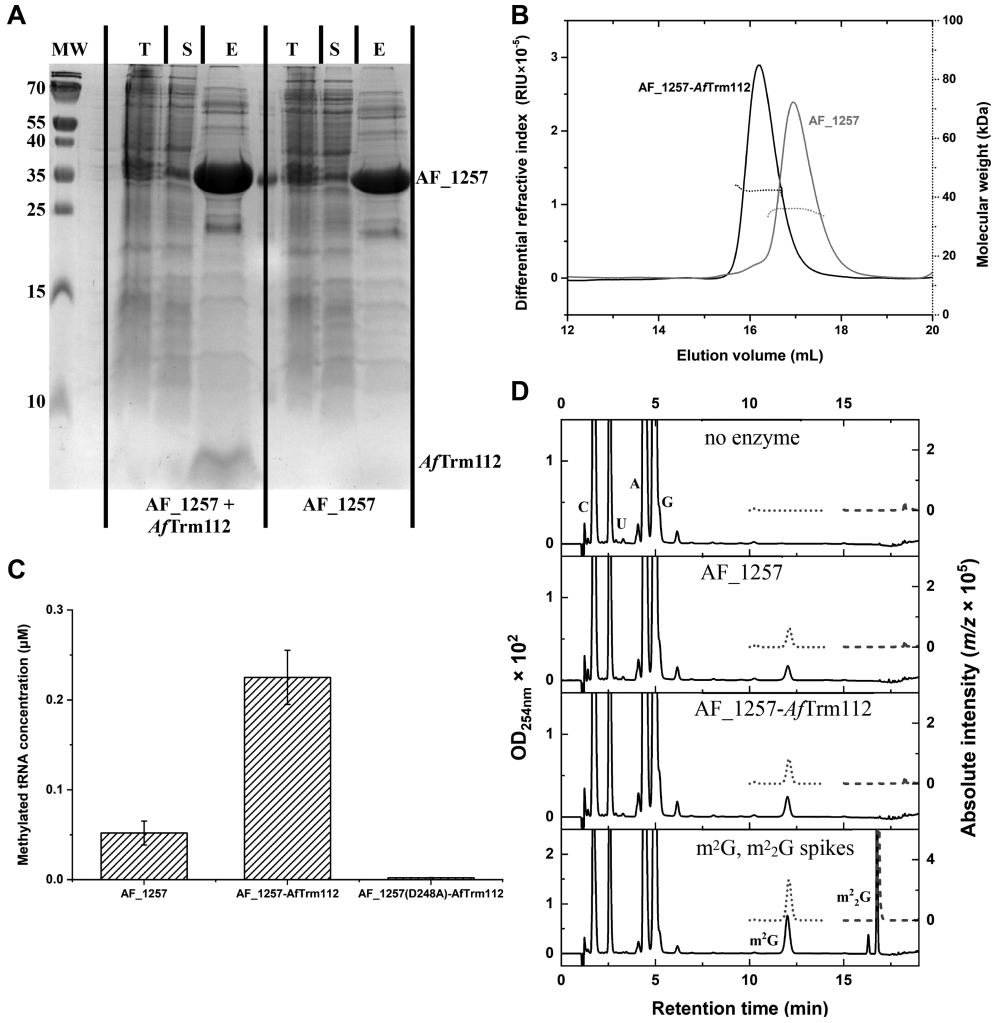

Figure 1. *Af*Trm112 stably interacts with AF_1257 and stimulates it. (**A**) AF_1257 does not require *Af*Trm112 to be expressed as a soluble protein in *E. coli*. AF_1257 protein was expressed alone or together with *Af*Trm112 in *E. coli* and subjected to micro-purification on NiNTA-agarose beads. Coomassie Blue stained SDS-PAGE analyses of proteins present in the total (T), soluble (S) and elution (E) fractions. A diffuse band below 10 kDa and corresponding to *Af*Trm112 (according to mass spectrometry) is only visible when AF_1257 is expressed with *Af*Trm112. (**B**). The AF_1257 protein physically interacts with *Af*Trm112. Chromatograms resulting from SEC-MALLS analysis of the AF_1257 protein (grey) and AF_1257-*Af*Trm112 complex (black). For the sake of clarity, only the main peak with the refractive index (solid lines, left y-axis) and the distribution of molecular mass calculated from light scattering along this peak (dashed lines, right y-axis) are shown. (**C**). Enzymatic assay of AF_1257 with or without *Af*Trm112 on *E. coli* $tRNA_i^{Met}$ *in vitro*. For each reaction (performed in triplicate), the corresponding proteins (3 pmol) were incubated at 65°C for 2 h with 75 pmol of tRNA in 50 μl of reaction system. (**D**). HPLC–MS elution profiles depicting the absorbance at 254 nm (left Y axis, solid lines) and the absolute intensity of m/z values of 298^+ (corresponding to m^2G protonated ion; right Y axis, dotted lines) and 312^+ (corresponding to $m^2{}_2G$ protonated ion; right Y axis, dashed lines) of the nucleosides digested from *E. coli* $tRNA_i^{Met}$ incubated in different conditions.

but its activity was around 5 times lower than that of the AF_1257-*Af*Trm112 complex after 2 h of reaction (Figure 1C). As already observed for several enzymes from hyperthermophilic organisms, the enzymatic activity was higher at 65°C than at 30°C (data not shown). Furthermore, the substitution by Ala of AF_1257 Asp248, which is located in a highly conserved signature known to be involved in recognition of the modified nucleotide, results in complete loss of enzymatic activity as previously observed for the corresponding D291A mutant from *S. cerevisiae* Trm11 (31). Both observations confirm that this enzymatic activity derives from AF_1257 and not from an *E. coli* tRNA MTase contaminant.

AF_1257 is an m^2G_{10} tRNA MTase

To determine the molecular function of AF_1257, *E. coli* $tRNA_i^{Met}$ was incubated with either AF_1257 or the AF_1257-*Af*Trm112 complex and hydrolyzed into nucleosides prior to HPLC–MS analyses. UV absorbance at 254 nm was recorded and specific ions were tracked by MS (m/z 298^+ and 312^+ for m^2G and $m^2{}_2G$ protonated species, respectively). Compared to the negative control (tRNA alone), the tRNAs incubated with either AF_1257 or the AF_1257-*Af*Trm112 complex exhibited a significant absorption peak in the 254 nm UV spectrum with a retention time between 12 and 12.5 min, which coincided with a strong signal at the m/z value expected for m^2G (Fig-

ure 1D). The identity of this peak as m^2G was further confirmed by a control experiment with digested unmodified tRNA sample spiked with commercial m^2G (Figure 1D). Although *Pab*Trm11 and *Tko*Trm11 were also shown to catalyze formation of $m^2{}_2G$ at position 10 of some tRNAs (37,38), we did not detect any signal for $m^2{}_2G$ (elution time around 16 to 17 min; Figure 1D). These experiments indicate that both AF_1257 and the AF_1257-*Af*Trm112 complex catalyze the formation of m^2G but not $m^2{}_2G$ on *E. coli* $tRNA_i^{Met}$ *in vitro*.

Next, due to (i) the presence of Trm14, an m^2G_6 tRNA MTase sharing the same domain organization as Trm11 in several archaea (58–60) and (ii) the presence of a G at position 6 in *E. coli* $tRNA_i^{Met}$ (Figure 2A), we mapped the m^2G modification on this tRNA to clarify whether AF_1257 is an m^2G_6 or an m^2G_{10} tRNA MTase. Control and modified $tRNA_i^{Met}$ were first digested by RNase A (which cleaves after pyrimidines) into oligonucleotides (Figure 2A), which were then analyzed by MALDI-TOF MS. The comparison of the spectra obtained for the samples incubated with either AF_1257 or the AF_1257-*Af*Trm112 complex to the spectrum of the control tRNA revealed a decrease in the intensity of the RNA fragment at *m/z* 1688.1 (unmodified oligonucleotide $_9GGAGC_{13}$) concomitantly with the appearance of the *m/z* value 1702.1 (Figure 2B). This indicates that the methyl group (+14 a.m.u shift) is added to the $_9GGAGC_{13}$ oligonucleotide. In contrast, the fragment at *m/z* 1721.1 corresponding to the $_4GGGGs^4U_8$ oligonucleotide remained unchanged in all these experiments, ruling out methylation at position 6 (Figure 2B). Additional fragmentation by MS/MS further revealed that the c2 (*m/z* 540.2) and d2 (*m/z* 558.2) ions lacking one base (either G_9 or G_{10}) also existed as a methylated species upon incubation with AF_1257 or AF_1257-*Af*Trm112 complex, indicating that the methyl group is added either on the G_9 or G_{10} ring (Figure 2C-D). As no methylated form of a1 (*m/z* 266.1) or c1 (*m/z* 346.1) ions (corresponding to G_9) were observed in tRNAs incubated with the enzymes, we conclude that the methylated nucleotide maps to position 10 (Figure 2C and E).

Altogether, these results demonstrate that AF_1257 (hereafter named *Af*Trm11) catalyzes the formation of m^2G_{10} on *E. coli* $tRNA_i^{Met}$ and hence, confirm that this protein is the orthologue of the archaeal *Pab*Trm11 and *Tko*Trm11 enzymes but also of *S. cerevisiae* Trm11.

The apo-, SFG- and Trm112-bound structures of AfTrm11

To obtain information on *Af*Trm11 and on the influence of *Af*Trm112 on its enzymatic activity, we determined the crystal structure of *Af*Trm11 in three different forms and at various resolutions, i.e. alone (2.75 Å resolution; one *Af*Trm11 copy in the asymmetric unit), bound to sinefungin (SFG; 1.9 Å; two *Af*Trm11 copies in the asymmetric unit) and as a complex with *Af*Trm112 and SFG (2.2 Å; one copy in the asymmetric unit; Table 1). The structure of the *Af*Trm11–Trm112 complex was solved using the multi-wavelength anomalous diffusion technique thanks to the anomalous signal of the zinc atom bound to *Af*Trm112, as previously done for some eukaryotic Trm112–MTase complexes (23,27). Then, the structure of *Af*Trm11 as determined in this complex was used to solve its apo- and SFG-bound structures by molecular replacement. All these *Af*Trm11 structures are virtually identical as revealed by their superimposition (rmsd values of 0.35–0.9 Å).

The *Af*Trm11 protein is composed of two domains: a N-terminal domain (hereafter named NTD; residues 1–140) separated from a C-terminal MTase domain (residues 154–320) by a short helical linker (residues 141–153; Figure 3A). The NTD domain is made of a curved 7 stranded β-sheet surrounded by three α-helices localized on the outer face of the β-sheet and can be further divided into two subdomains: the NFLD (for N-terminal Ferredoxin like domain; residues 1–66) and the core THUMP domain (named after THioUridine synthase, MTase and Pseudouridine synthase (61); residues 67–140; Figure 3A and Supplementary Figure S2A). The MTase domain adopts a typical class-I SAM-dependent MTase fold composed of a seven stranded β-sheet surrounded by three α-helices on one side and one on the other side (Figure 3A and Supplementary Figure S2B). This domain harbors the conserved $_{248}DYPY_{251}$ motif, which corresponds to the [N/D/S]-P-[P/I]-[Y/F/W/H] signature commonly found in MTases modifying planar amino groups from DNA, RNA or proteins (62–64). Overall, this modular organisation is very similar to that of the previously solved *Tko*Trm11 structure (38).

In the *Af*Trm11-SFG structure, SFG binds in an unconventional manner within the SAM binding site as revealed by comparison with the structures of *Tko*Trm11 bound to SAM ((38); Figure 3B) and of archaeal *P. furiosus* Trm14 (59), another tRNA modification enzyme with the same THUMP-MTase modular organisation, bound to SFG. Indeed, while the adenosine rings from SAM and SFG interact in their conventional pocket, the amino acyl group from SFG points in the opposite direction compared to the L-methionine moiety from SAM (Figure 3B). The comparison of *Af*Trm11 apo- and SFG-bound forms reveals that while the loop containing residues 254–258, which is located just upstream of the $_{248}DYPY_{251}$ motif could not be modeled due to intrinsic flexibility in the structure of the *Af*Trm11 apo-form, this loop is structured in the *Af*Trm11-SFG complex due to its involvement in crystal packing (Supplementary Figure S3A). Similarly, upon SFG binding, the aromatic ring from Phe206 slightly rotates so as to form a π–π stacking with the adenine base of SFG (Supplementary Figure S3A).

The structure of the *Af*Trm11–Trm112 complex bound to SFG reveals that *Af*Trm112 is made of a single domain (ZBD for zinc binding domain) composed of an α-helix (α1) packed onto a 4 stranded anti-parallel β-sheet and adopts the same fold as *H. volcanii* Trm112 (Figure 3A and Supplementary Figure S4, rmsd value of 0.75 Å over 57 Cα atoms and 56% sequence identity; (36)). Similarly to fungal Trm112 proteins, this protein binds one zinc atom through four cysteine residues that are strongly conserved in fungal and to a lesser extent in archaeal Trm112 proteins (Supplementary Figure S4; (18,22,23,27)). In the *Af*Trm11–Trm112 complex, SFG adopts the same conformation as in the structure of *Af*Trm11. Further comparison of the *Af*Trm11 and *Af*Trm11–Trm112 SFG-bound forms does not reveal major conformational changes despite the binding of *Af*Trm112 in the vicinity of the SAM

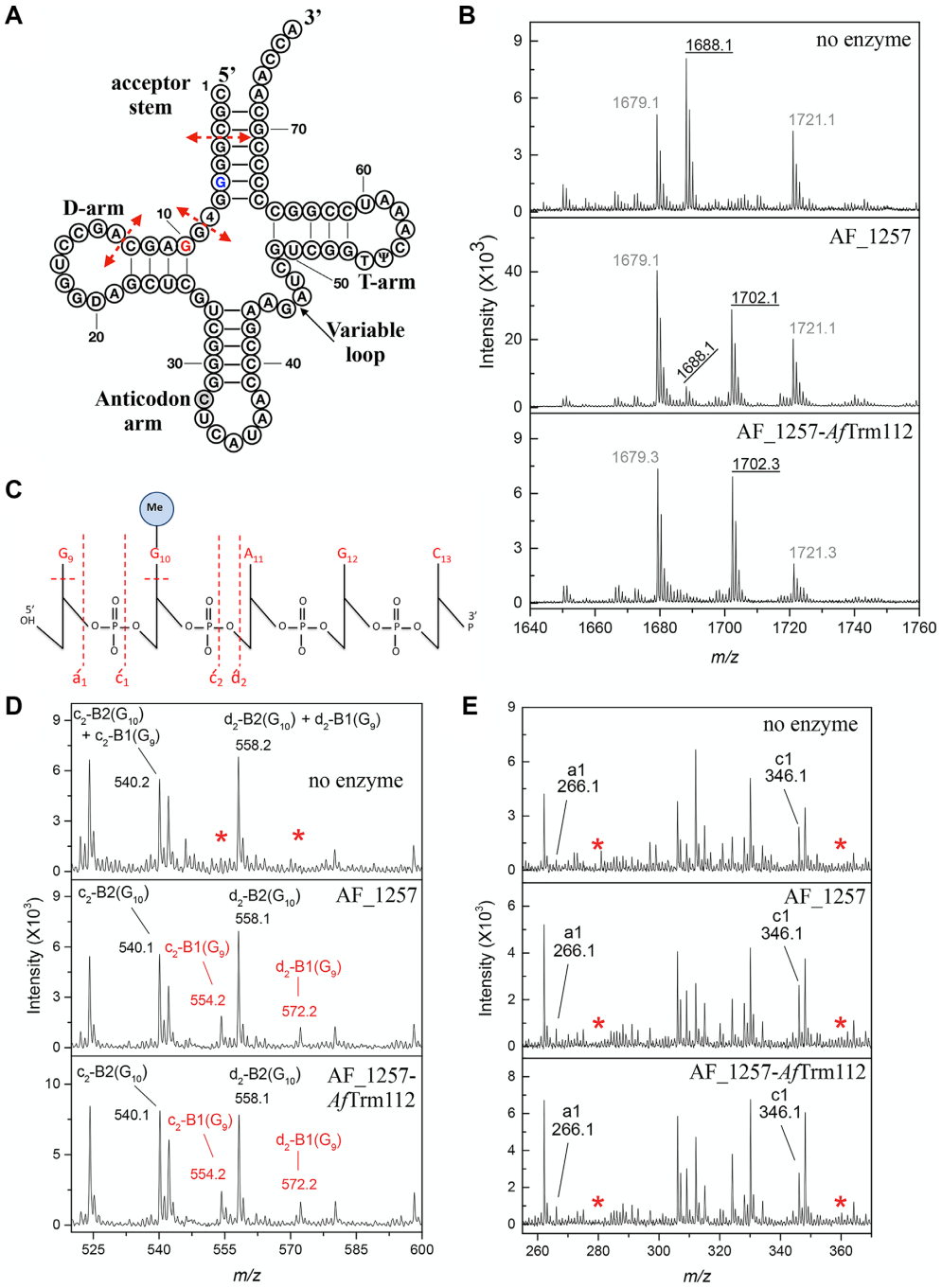

Figure 2. The AF_1257-*Af*Trm112 complex is an m^2G_{10} tRNA methyltransferase. (**A**) Clover-leaf representation of *E. coli* $tRNA_i^{Met}$ with the RNase A cleavage sites of interest for this study shown as red dashed lines. Positions G_6 and G_{10} are highlighted in blue and red, respectively. Position C32, which is 2'-OH methylated (Cm) in *E. coli* $tRNA_i^{Met}$ is highlighted in gray. 4, T and Ψ stand for 4-thiouridine, thymidine and pseudouridine, respectively. (**B**) MALDI-TOF MS spectrum of $_9GGAGC_{13}$ oligonucleotide obtained upon digestion with RNase A of *E. coli* $tRNA_i^{Met}$ following incubation with either MTase buffer (upper panel), AF_1257 (middle panel) or AF_1257-A*f*Trm112 (lower panel). (**C**) Discussed a-, c- and d-type fragment ions for the $_9GGAGC_{13}$ oligonucleotide upon digestion of the *E. coli* $tRNA_i^{Met}$ by RNase A. This nomenclature is based on McLuckey *et al.* (73). (**D**) CID Spectrum of the c2- and d2-type fragment ions lacking one base observed in *E. coli* $tRNA_i^{Met}$ incubated with MTase buffer (upper panel), AF_1257 (middle panel) or AF_1257-A*f*Trm112 (lower panel). The expected position of methylated ions is depicted by a red asterisk. (**E**) CID Spectrum of the a1- and c1-type fragment ions observed in *E. coli* $tRNA_i^{Met}$ incubated with MTase buffer (upper panel), AF_1257 (middle panel) or AF_1257-A*f*Trm112 (lower panel). The expected position of methylated ions is depicted by a red asterisk.

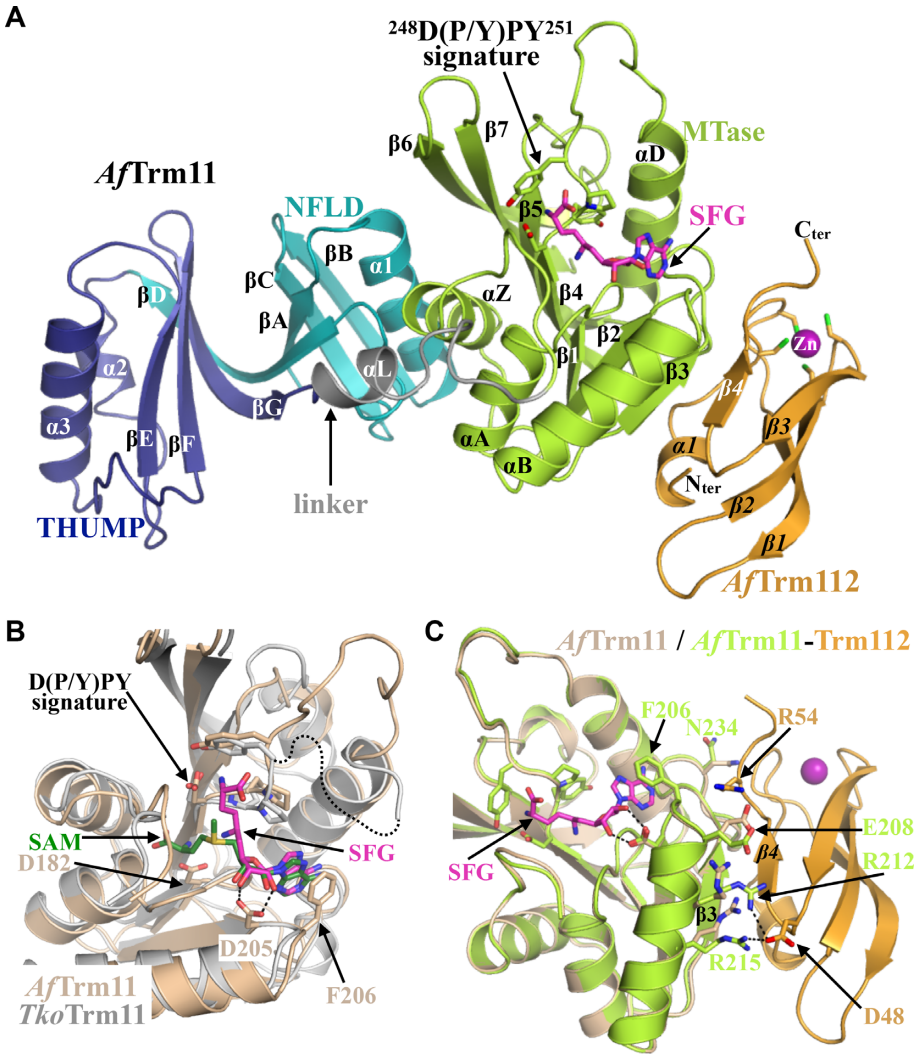

Figure 3. Structure of the *Af*Trm11-Trm112 complex. (**A**) Cartoon representation of the *Af*Trm11-Trm112 complex bound to sinefungin (SFG). NFLD, THUMP and MTase domains from *Af*Trm11 are colored in dark blue, blue and light green, respectively. The linker connecting the N-terminal domain (NFLD + THUMP) to the C-terminal MTase domain is colored in gray. *Af*Trm112 is colored in light orange. The zinc atom bound to *Af*Trm112 is depicted as a purple sphere and side chains from the cysteine residues coordinating this zinc atom are shown as sticks. The DYPY signature from the MTase domain is shown as sticks. SFG is colored in magenta. Secondary structure elements from *Af*Trm112 are labeled in italics. With the exception of Figure 4E, all figures illustrating structural aspects have been generated using the Pymol software (74). (**B**) Sinefungin binds in an unconventional manner. The superimposition of *Af*Trm11 (beige) bound to SFG (magenta) onto *T. kodakarensis* Trm11 (gray; PDB code: 5E72) bound to SAM (grey) reveals that the amino acid moiety of SFG does not bind to the classical pocket involved in the recognition of L-methionine from SAM. The loop corresponding to residues 250–260 from AfTrm11 is also not defined in the crystal structure of *T. kodakarensis* Trm11 and is depicted as a black dashed line. Hydrogen bonds are highlighted by dashed black lines. (**C**) Binding of *Af*Trm112 has no major structural influence on *Af*Trm11 regions involved in SAM recognition or *Af*Trm112 interaction. *Af*Trm11 side chains from the interface adopting different conformations upon *Af*Trm112 binding are shown as sticks. *Af*Trm112 residues facing them are also shown as sticks.

binding site (Figure 3C). This suggests that *Af*Trm112 does not influence the conformation of the SAM binding site. Next, we compared the affinity of *Af*Trm11 and *Af*Trm11–Trm112 for SAM by ITC experiments at 50°C and found that *Af*Trm112 has little to no influence on the affinity of *Af*Trm11 for SAM, in agreement with our structural observation (Supplementary Figure S5; Table 2). This is in striking contrast with the strict Trm112 requirement of *S. cerevisiae* Trm11 for SAM binding (31).

This first crystal structure of a Trm11-Trm112 complex shows that Trm112 exclusively contacts the MTase domain from Trm11 through an interface area of 900 Å^2 (Figure 3A and C). This interface relies on the formation of a β-zipper formed by two hydrogen bonds between main chain atoms from strand β3 from the *Af*Trm11 MTase domain and strand β4 from *Af*Trm112 (Supplementary Table S3). A total of 22 amino acids from *Af*Trm11 interact with 17 amino acids from *Af*Trm112, respectively (Supplementary Figure S3B-D). The core of the interface is enriched in hydrophobic residues (Ile202, Val201, Val227, Leu228, Leu229, Leu28, Leu237 and Val 242 from *Af*Trm11 and Leu5, Leu9, Ala10, Ile50, Pro51 and Leu53 from *Af*Trm112) while the outer shell is mainly composed of polar residues forming hydrogen bonds as well as three salt bridges (Supplementary Fig-

Table 2. Thermodynamics parameters for SAM binding at 50°C as determined by ITC

	K_d (μM)	Stoechiometry (*n*)	Δ*H* (kcal/mol)	*T*Δ*S* (kcal/mol)
***Af*Trm11**	11.4 ± 3.4	0.72	-4.54	0.43
***Af*Trm11–Trm112**	8.26 ± 2.43	0.83	-3.77	0.58

ure S2, S3B-D and S4; Supplementary Table S3). Furthermore, with the exception of slight side chain rearrangements of *Af*Trm11 (Supplementary Figure S3E), binding of *Af*Trm112 has no major consequences on the *Af*Trm11 structure. Overall, the structure of the Trm11–Trm112 complex, the last Trm112–MTase complex that was resistant to crystallization before this study, shows that this interaction mode is highly reminiscent of previously solved crystal structures of archaeal and eukaryotic Trm112-MTase complexes (18,20,23,27,36,65,66).

From our analyses, *Af*Trm112 has no structural impact on *Af*Trm11 or on SAM binding. Therefore, we have characterized the kinetics parameters of *Af*Trm11 alone or as a complex with *Af*Trm112 to understand the stimulating effect of *Af*Trm112 on the *Af*Trm11 enzymatic activity (Supplementary Figure S5C–F and Table 3). The *Af*Trm11 protein alone displays stronger affinity (13-fold) for *E. coli* $tRNA_i^{Met}$ but exhibits a lower k_{cat} (almost 7-fold) than the *Af*Trm11–Trm112 complex. This indicates that *Af*Trm112 significantly stimulates the catalytic step of the reaction at the expense of tRNA binding. Altogether, combining structural and biochemical characterization, we show that *Af*Trm112 strongly enhances the enzymatic activity of *Af*Trm11 by improving its stability (according to the behavior of this protein during purification and to a thermal shift assay) and mostly the catalytic step of the methylation reaction so as to achieve an optimal enzymatic efficiency.

DISCUSSION

tRNAs are by far the most post-transcriptionally modified nucleic acids. The biological importance of many of those modifications is becoming increasingly evident for organism development, as mutants affecting the activity of many tRNA modification enzymes are being identified in patients suffering from intellectual disorders or cancers. Most of these enzymes are also conserved between domains of life and in particular between eukaryotes and archaea, emphasizing their functional importance. Here, we have focused on the Trm11 protein from *A. fulgidus* (*Af*Trm11), an archaeon living in a sulfur-rich environment and whose optimal growth temperature is 83°C. We anticipate that similarly to the *T. kodakarensis TRM11* gene (44,45), the *AF_1257* gene encoding for *Af*Trm11 is required for cellular fitness and adaptation at high temperature. We have characterized the enzymatic activity of this protein as an MTase catalyzing the formation of m^2G at position 10 of tRNAs (Figures 1D and 2). One major difference between archaeal and eukaryotic Trm11 enzymes is the inability of the latter enzymes to catalyse the formation of $m^2{}_2G_{10}$ (30,67). In archaea, both m^2G_{10} and $m^2{}_2G_{10}$ have been identified in tRNAs extracted from *Halobacterium salinarum*, *H. volcanii*, *Sulfolobus acidocaldarius* and *T. kodakarensis* (40,45,67,68), while *Pab*Trm11 and *Tko*Trm11 enzymes were shown to catalyse the formation of these two modifications (37,38). In our experimental conditions, coupling LC/MS and MS/MS analyses, we detected m^2G_{10} but no $m^2{}_2G_{10}$ in the *E. coli* $tRNA_i^{Met}$ used in our assay upon incubation with the *Af*Trm11 protein (Figures 1D and 2). In the absence of information regarding *A. fulgidus* total tRNA modifications, we cannot exclude that tRNAs from this organism exclusively contain the m^2G_{10} modification. However, in the case of *Pab*Trm11, the presence of U at position 25 and a four nucleotide long V-loop are required for formation of $m^2{}_2G_{10}$ in archaeal tRNAs (39). It is then likely that the presence of a C at position 25 (which base pairs with G_{10} in the tRNA structure, Figure 2A) of the *E. coli* $tRNA_i^{Met}$ is responsible for the mono-methylation but not dimethylation that we observe with this substrate. We hence do not exclude that this enzyme also catalyzes the formation of $m^2{}_2G_{10}$ on other tRNA species that have not been tested in our study.

On the importance of *Af*Trm112 for *Af*Trm11 activity

Here, we demonstrated for the first time that when a Trm112 orthologue is present in the archaeal genome, it interacts directly with Trm11 (Figure 1B), confirming co-immunoprecipitation of *H. volcanii* Trm11 with Trm112 (36). We also showed that Trm112 is important but not mandatory for Trm11 activity. Indeed, similarly to Trm11 enzymes from *P. abyssii* and *T. kodakarensis* archaea (37,38), *Af*Trm11 was active on its own but its enzymatic activity was significantly enhanced by Trm112 (Figure 1C), a well-known allosteric activator of several eukaryotic MTases modifying tRNAs (including Trm11), rRNAs and the translation termination factor eRF1 (16). We observed that *Af*Trm112 protects *Af*Trm11 from thermal denaturation by increasing its Tm value (Supplementary Figure S1 and Table S2). Although Tm values measured *in vitro* in a specific buffer imperfectly reflect the stability of a protein in its cellular environment, we anticipate that *Af*Trm112 might play a crucial a role *in vivo* by stabilizing *Af*Trm11 in the *A. fulgidus* archaeon, whose optimal growth temperature is 83°C. Our detailed analysis aimed at clarifying the role of *Af*Trm112 in the activation of *Af*Trm11 reveals that both *Af*Trm11 and *Af*Trm11–Trm112 have similar affinities for SAM (Supplementary Figure S5A. B). This correlates with our co-crystal structures of *Af*Trm11-Trm112 and of *Af*Trm11, both bound to SFG, a competitive inhibitor of SAM-dependent MTases (Figure 3), which revealed no significant changes in the *Af*Trm11 SAM binding site upon *Af*Trm112 binding. In addition, our different crystal structures of *Af*Trm11 obtained in the absence or the presence of *Af*Trm112 do not highlight significant changes in the *Af*Trm11 active site upon *Af*Trm112 binding. This suggests that the activation role of *Af*Trm112 is not

Table 3. Kinetics parameters

	K_m for tRNA (μM)	k_{cat} for tRNA (min^{-1})	k_{cat}/K_m ($\mu M^{-1}.min^{-1}$)
***Af*Trm11**	0.089 ± 0.013	0.126 ± 2.25*10^{-3}	1.42
***Af*Trm11–Trm112**	1.18 ± 0.193	0.883 ± 0.05	0.75

through the molding of the *Af*Trm11 active site into a form competent for the coordination of G_{10} (Figure 3C). However, we have clearly shown that *Af*Trm112 significantly enhances the catalytic step of the tRNA methylation reaction at the expense of a decreased affinity for tRNA (Table 3 and Supplementary Figure S5C–F). Hence, contrary to its eukaryotic orthologues, we have no evidence that *Af*Trm112 activation mode relies on an allosteric effect. Several non exclusive possibilities can explain how *Af*Trm112 activates *Af*Trm11. First, it may contribute to the correct positioning of the substrate in the tRNA binding site so as to orient properly the guanine at position 10 into the enzyme active site. Second, it could help the *Af*Trm11 catalytic subunit to flip out G_{10} from the tRNA core to increase its accessibility. Indeed, the lower Km for tRNA measured for *Af*Trm11 (K_m of 88.5 nM) compared to the *Af*Trm11-Trm112 complex (K_m of 1.18 μM) may reflect the formation of a nonproductive enzyme-substrate complex. Unfortunately, despite extensive trials, we could not obtain the crystal structure of *Af*Trm11 or *Af*Trm11-Trm112 bound to a tRNA substrate. Third, our observation that the amount of tRNA modified (2.5 pmol) by *Af*Trm11 is slightly lower than the enzyme quantity (3 pmol) could indicate that in the absence of *Af*Trm112, *Af*Trm11 cannot perform several catalytic cycles and remains tightly bound to its product. Hence, *Af*Trm112 could assist *Af*Trm11 in the release of the reaction product (see below). Finally, another explanation for the stimulating role of *Af*Trm112 on *Af*Trm11 enzymatic activity could be that the latter is much less stable in the absence of *Af*Trm112, as we previously experienced with *S. cerevisiae* Trm11 (Supplementary Figure S1 and Table S2; (31)). Indeed, at the temperature (65°C) and buffer condition used in our enzymatic assays, we cannot exclude that in the absence of *Af*Trm112, a significant portion of *Af*Trm11 starts to unfold (Tm of the protein alone is 72.8°C in the MTase buffer), resulting in lower enzymatic activity. Furthermore, the analysis of the *Af*Trm11 surface interacting with *Af*Trm112 reveals the presence of a central area exclusively composed of hydrophobic residues, which is shielded from the solvent upon complex formation with *Af*Trm112 (Supplementary Figure S6, left). In comparison, the corresponding region from *Tko*Trm11 harbors two hydrophilic residues (Thr230 and Lys232) at the heart of this hydrophobic core, thereby probably increasing its solubility and its stability (Supplementary Figure S6, right). Furthermore, the loop connecting strands β3 to β4, which is involved in the interaction between *Af*Trm11 and *Af*Trm112, is longer in *Tko*Trm11, resulting in the presence of a short 3_{10} helix that projects Asp241 (Glu241 in *Pab*Trm11) towards the solvent (Supplementary Figures S2B and S6, right). Both observations could explain why *Tko*Trm11 and *Pab*Trm11 proteins do not require a Trm112 orthologue for optimal activity, contrary to *Af*Trm11.

Implications for tRNA binding

Despite extensive efforts, we could not determine the crystal structure of the complex between *E. coli* $tRNA_i^{Met}$ and either *Af*Trm11 or the *Af*Trm11-Trm112 complex. We then compared our structure of the *Af*Trm11-Trm112 complex to those of two m^2G (RsmC) or $m^2{}_2G$ (TGS1) MTases solved in the presence of a guanosine moiety in their active sites (69,70). Indeed, the structure of human TGS1, an $m^2{}_2G$ MTase modifying the m^7G cap present at the 5′ end of small nuclear and small nucleolar RNAs, of the telomerase RNA and of some mRNAs, has been determined in the presence of both m^7GTP and SAH (*S*-adenosyl-*L*-homocysteine, the product regenerated upon transfer of the SAM methyl group onto its substrate; (70)). Similarly, the structure of the *T. thermophilus* RsmC protein, which modifies 16S rRNA on G_{1207}, a nucleotide located near the decoding center in the 30S small ribosomal subunit, to form m^2G_{1207} (71), has been determined in complex with SAM and guanosine (69). These three enzymes share the [N/D/S]-P-[P/I]-[Y/F/W/H] active site signature known to coordinate the planar amino group to be modified and their MTase domain are closely related from a structural point of view (rmsd values of 1.5–1.6 Å). Interestingly, in both TGS1 and RsmC, the guanosine rings are stacked in a parallel manner onto the aromatic ring of the fourth residue of the active site signature. However, these rings are in orthogonal conformations relative to the [N/D/S]-P-[P/I]-[Y/F/W/H] signature (Figure 4A, B). In the RsmC-SAM-guanosine complex (Figure 4A), the N^2 atom from the guanine ring is 4.7 Å away from the SAM methyl group, which is not compatible with methyl transfer via the SN_2 mechanism commonly accepted for this family of MTases. Hence, the guanosine position trapped in this crystal structure is unlikely to be in its correct orientation. Indeed, this structure was obtained by co-crystallizing the enzyme in the presence of both substrates (SAM and guanosine) and hence, if the guanosine ring had been correctly positioned in the active site, one would expect that the methylation would have occurred, resulting in the presence of SAH and m^2G in the active site instead of SAM and guanosine. On the contrary, modeling a SAM molecule in the TGS1-SAH-m^7GTP structure reveals a distance of 3 Å between the SAM methyl group and the N^2 atom from the m^7GTP cap (Figure 4B). Hence, the coordination of the guanine ring as observed in human TGS1 structure is more likely to reflect the correct location of the substrate in the active site of m^2G or $m^2{}_2G$ MTases. More detailed comparison of TGS1 and *Af*Trm11 active sites further reveals that the loop preceding helix αZ from *Af*Trm11 might, together with Tyr251 side chain, sandwich the guanine ring as helix α4 and Trp766 do in TGS1 (Figure 4B). In addition, the side chain from the strictly conserved Arg313 in *Af*Trm11 is in the same region as Arg807 and Lys836 from TGS1 (Figure 4B, Supplemen-

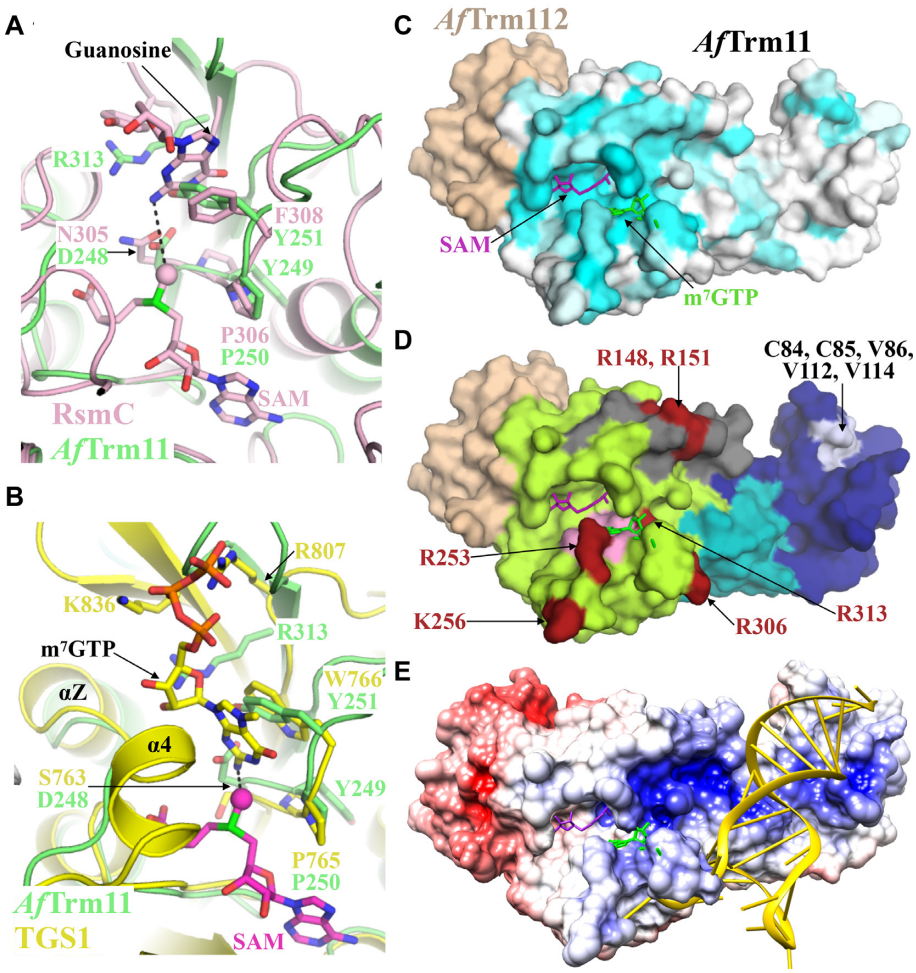

Figure 4. Implications for tRNA recognition. (**A**) Comparison of *Af*Trm11 (light green) and RsmC (light pink) active sites. The SAM and guanosine molecules bound to RsmC are shown as pink sticks. In panels A and B, the SAM methyl group to be transferred is shown as a sphere and the distance between this methyl group and the N^2 atom to be methylated on guanosine is shown by a dashed black line. (**B**) Comparison of *Af*Trm11 (light green) and human TGS1 (yellow) active sites. The SAM molecule (magenta sticks) has been modeled by superimposing coordinates of SAM onto those of the SAH molecule bound to TGS1. The m^7GTP molecule bound to TGS1 is shown as yellow sticks. (**C**) Sequence conservation mapped at the surface of the *Af*Trm11–Trm112 complex. The conservation score for Trm11 proteins was calculated using the CONSURF server (75). *Af*Trm112 is colored in beige. Sequence conservation score is represented as a gradient of white (no conservation) to cyan (high conservation) at the surface of *Af*Trm11. The same orientation of the complex is used for panels C to E. (**D**) Functionally important residues are spread at the surface of *Af*Trm11. Residues important for the enzymatic activity of archaeal Trm11 proteins are mapped in white on THUMP domains and in red wine in the linker region and MTase domain. The NYPY active site signature is colored pink. *Af*Trm11 domains are colored using the same color code as Figure 3A. *Af*Trm112 is colored in beige. (**E**) A long positively charged groove can accommodate the tRNA. Positively charged (10 k_BT/e^-) and negatively charged (-10 k_BT/e^-) regions are colored in blue and red, respectively. The electrostatic potential was calculated using APBS program as implemented in the Chimera software (76). An aminoacyl acceptor arm (yellow) was modeled by superimposing the structure of the THUMP domain from the 4-thiouridine synthetase ThiI bound to the aminoacyl acceptor arm of the *E. coli* $tRNA^{Phe}$ (PDB code: 4KR6; (42)) onto the structure of *Af*Trm11 THUMP domain.

tary Figure S2B). As these residues contact the phosphate groups of the m^7GTP cap, Arg313 is very likely to interact with the phosphate backbone of the tRNA substrate.

Further analyses show that the *Af*Trm11 active site, encompassing the $_{248}$DYPY$_{251}$ signature and Arg313, is the most conserved region accessible at the surface of the complex (Figure 4C). *Af*Trm11 residues (Arg 148, Arg151, Arg253, Lys256 or Arg306) correspond to *Tko*Trm11 residues that were shown to be important for catalysis and tRNA binding (Lys151, Arg152, Arg266, Lys267, Arg268 and Arg317; Figure 4D; (38)). We then anticipate that those residues are very likely to be important for tRNA binding and in particular to coordinate G_{10} in *Af*Trm11 active site. A positively charged groove running from the NTD to the active site is very likely to interact with the tRNA backbone. Adjacent to this positively charged region, the surface formed by Cys84, Cys85, Val86, Val112 and Val114 from the *Af*Trm11 THUMP subdomain matches that formed by Phe86, Lys87, Val88, Val118 and Leu120 in *Tko*Trm11, residues that were shown to be important for tRNA recognition (Figure 4D-E). The equivalent regions in the ThiI THUMP domain directly interact with the amino acyl acceptor arm and in particular the CCA motif present at the 3′ end of mature tRNAs. This is in agreement with earlier observations that the enzymatic activity of both eukaryotic and archaeal Trm11 proteins is reduced on tRNA sub-

strates lacking this CCA motif (31,38). Altogether, those observations explain why both domains from *Pab*Trm11 are required for enzymatic activity (41). Very interestingly, *Af*Trm112 contributes a negatively charged region at the surface of the *Af*Trm11–Trm112 complex (Figure 4E). As this region is close to the *Af*Trm11 active site, it is likely to repel the negatively charged tRNA substrate, thereby rationalizing the lower Km of the *Af*Trm11-Trm112 complex for tRNA compared to *Af*Trm11 alone (Table 3). This further suggests that one of *Af*Trm112 functions is to favor product release to allow several catalytic cycles thereby enhancing the k_{cat} of the enzyme (Table 3).

Finally, the structures of four m^2G MTases with the same modular organization, *i.e.* a NTD composed of a NFLD and a THUMP subdomain fused to a MTase domain, are now available: the *Af*Trm11 and *Tko*Trm11 $m^2G/m^2{}_2G$ MTases as well as those of two TrmN/Trm14 m^2G_6 MTases from either bacteria (TrmN from *Thermus thermophilus*) or archaea (Trm14 from *P. furiosus*; this work and (38,59)). This offers the opportunity to analyse the intrinsic flexibility between these two domains. Interestingly, as observed for the structures of TrmN and Trm14 (overall rmsd values of 0.35–2.0 Å over 286 Cα atoms; (59)), the comparison between several archaeal Trm11 structures (3 for *Af*Trm11 obtained in different space groups and hence crystal packing as well as one for *Tko*Trm11) does not reveal striking differences in the orientation of the NTD relative to the MTase domain in Trm11 enzymes (overall rmsd values of 0.5–1.2 Å over 304 Cα atoms), indicating that these two domains most likely behave as a single rigid unit. So, this observation seems to invalidate our former proposal that in the yeast Trm11–Trm112 complex (31), the NTD may move relative to the MTase domain to bring the G_{10} nucleotide into the Trm11 MTase active site. This new analysis rather suggests that the tRNA may first interact through its aminoacyl acceptor arm with the Trm11 NTD and then kink to bring the region containing G_{10} into the active site. This might be favored by an incomplete set of modifications within Trm11 tRNA substrates, which may increase their intrinsic flexibility. Indeed, a recent study aimed at monitoring the addition of tRNA modifications using yeast cell extracts revealed that many of those occur in the T-arm, either concomitantly with m^2G_{10} or even later (72). This model further supports the ruler model first proposed for ThiI and then for Trm11 and TrmN/Trm14 MTases (38,42). Indeed, this latter model posits that the orientation of the THUMP domain relative to the MTase domain defines the distance between the tRNA CCA extremity and the nucleotide to be modified. In Trm11, the distance between the residues from the region of the NTD supposed to interact with the 3′-OH extremity of the tRNA (Cys85 in *Af*Trm11 and Lys87 in *Tko*Trm11) and the SAM methyl group is around 45 Å and hence corresponds to the distance between the N^2 atom from G_{10} and the 3′-OH extremity of a mature tRNA (47 Å). The same is true in the structures of TrmN/Trm14 MTases.

CONCLUSION

In conclusion, we have studied the tRNA modification enzyme Trm11 from the *A. fulgidus* archaeon, revealing that this protein can be considered as a missing link between some archaeal Trm11 enzymes, which are active on their own, and eukaryotic ones, which are strictly dependent on the Trm112 activator. Indeed, although *Af*Trm11 exhibits some enzymatic activity, this activity is strongly enhanced in the presence of *Af*Trm112. We have also determined the crystal structures of *Af*Trm11 bound to *Af*Trm112 and to sinefungin (SFG), a SAM-dependent MTase inhibitor. This structure is the first one of a complex between Trm112 and Trm11, for which so far structural information could only be obtained by a combination of molecular modeling and hydrogen-deuterium exchange experiments coupled to mass spectrometry measurements (31).

SUPPLEMENTARY DATA

Supplementary Data are available at NAR Online.

ACKNOWLEDGEMENTS

We are grateful to the SOLEIL staff for smoothly running the facility. Experiments were performed on the Proxima-2A beamline at SOLEIL Synchrotron, France (proposal numbers 20160821, 20170871 and 20181001). We are indebted to Dr Yves Mechulam and Dr Emmanuelle Schmitt for the kind gift of the plasmid for the expression of *E. coli* $tRNA_i^{Met}$ and for their advices in purifying this tRNA. We are also grateful to Dr Damien Brégeon and Dr Dominique Liger for helpful discussion regarding tRNA preparation for MALDI-MS/MS analyses and enzymatic studies. We are indebted to Pr. Thomas Simonson for critical reading of this manuscript.
Author contributions: C.W., T.V.N. and M.G. designed research. C.W., T.V.N., V.J., V.G. and M.G. performed and analyzed the experiments. C.W and M.G. wrote the paper.

FUNDING

M.G. acknowledges financial supports from the Centre National pour la Recherche Scientifique (CNRS); Agence Nationale pour la Recherche (ANR) [ANR-14-CE09-0016-02]; Ecole Polytechnique; C.W. is a recipient of fellowship from the Chinese Scholarship Council (CSC) and T.V.N. was supported by a PhD fellowship from the French Ministère de l'Enseignement Supérieur et de la Recherche (MESR); TVN was also supported by a mini post-doc fellowship from Ecole Polytechnique. Funding for open access charge: CNRS.
Conflict of interest statement. None declared.

REFERENCES

1. Tarrant,D. and von der Haar,T. (2014) Synonymous codons, ribosome speed, and eukaryotic gene expression regulation. *Cell. Mol. Life Sci.*, **71**, 4195–4206.
2. Nedialkova,D.D. and Leidel,S.A. (2015) Optimization of codon translation rates via tRNA modifications maintains proteome integrity. *Cell*, **161**, 1606–1618.
3. Ranjan,N. and Rodnina,M.V. (2016) tRNA wobble modifications and protein homeostasis. *Translation (Austin)*, **4**, e1143076.
4. Motorin,Y. and Helm,M. (2010) tRNA stabilization by modified nucleotides. *Biochemistry*, **49**, 4934–4944.
5. Agris,P.F., Narendran,A., Sarachan,K., Vare,V.Y.P. and Eruysal,E. (2017) The importance of being modified: the role of RNA modifications in translational fidelity. *The Enzymes*, **41**, 1–50.

6. Putz,J., Florentz,C., Benseler,F. and Giege,R. (1994) A single methyl group prevents the mischarging of a tRNA. *Nat. Struct. Biol.*, **1**, 580–582.
7. Maraia,R.J. and Arimbasseri,A.G. (2017) Factors that shape eukaryotic tRNAomes: processing, modification and anticodon-codon use. *Biomolecules*, **7**, 26.
8. Prabhakar,A., Choi,J., Wang,J., Petrov,A. and Puglisi,J.D. (2017) Dynamic basis of fidelity and speed in translation: Coordinated multistep mechanisms of elongation and termination. *Protein Sci.*, **26**, 1352–1362.
9. Powell,C.A., Nicholls,T.J. and Minczuk,M. (2015) Nuclear-encoded factors involved in post-transcriptional processing and modification of mitochondrial tRNAs in human disease. *Front. Genet.*, **6**, 79.
10. Bednarova,A., Hanna,M., Durham,I., VanCleave,T., England,A., Chaudhuri,A. and Krishnan,N. (2017) Lost in translation: defects in transfer RNA modifications and neurological disorders. *Front. Mol. Neurosci.*, **10**, 135.
11. Braun,D.A., Rao,J., Mollet,G., Schapiro,D., Daugeron,M.C., Tan,W., Gribouval,O., Boyer,O., Revy,P., Jobst-Schwan,T. *et al.* (2017) Mutations in KEOPS-complex genes cause nephrotic syndrome with primary microcephaly. *Nat. Genet.*, **49**, 1529–1538.
12. Pereira,M., Francisco,S., Varanda,A.S., Santos,M., Santos,M.A.S. and Soares,A.R. (2018) Impact of tRNA modifications and tRNA-modifying enzymes on proteostasis and human disease. *Int. J. Mol. Sci.*, **19**, 3738.
13. Guy,M.P. and Phizicky,E.M. (2014) Two-subunit enzymes involved in eukaryotic post-transcriptional tRNA modification. *RNA Biol*, **11**, 1608–1618.
14. Thiaville,P.C., Iwata-Reuyl,D. and de Crecy-Lagard,V. (2014) Diversity of the biosynthesis pathway for threonylcarbamoyladenosine (t(6)A), a universal modification of tRNA. *RNA Biol*, **11**, 1529–1539.
15. Karlsborn,T., Tukenmez,H., Mahmud,A.K., Xu,F., Xu,H. and Bystrom,A.S. (2014) Elongator, a conserved complex required for wobble uridine modifications in eukaryotes. *RNA Biol* **11**, 1519–1528.
16. Bourgeois,G., Letoquart,J., van Tran,N. and Graille,M. (2017) Trm112, a protein activator of methyltransferases modifying actors of the eukaryotic translational apparatus. *Biomolecules*, **7**,7.
17. Figaro,S., Wacheul,L., Schillewaert,S., Graille,M., Huvelle,E., Mongeard,R., Zorbas,C., Lafontaine,D.L. and Heurgue-Hamard,V. (2012) Trm112 is required for Bud23-mediated methylation of the 18S rRNA at position G1575. *Mol. Cell. Biol.* **32**, 2254–2267.
18. Letoquart,J., Huvelle,E., Wacheul,L., Bourgeois,G., Zorbas,C., Graille,M., Heurgue-Hamard,V. and Lafontaine,D.L. (2014) Structural and functional studies of Bud23-Trm112 reveal 18S rRNA N7-G1575 methylation occurs on late 40S precursor ribosomes. *Proc. Natl. Acad. Sci. U.S.A.*, **111**, E5518–E5526.
19. Zorbas,C., Nicolas,E., Wacheul,L., Huvelle,E., Heurgue-Hamard,V. and Lafontaine,D.L. (2015) The human 18S rRNA base methyltransferases DIMT1L and WBSCR22-TRMT112 but not rRNA modification are required for ribosome biogenesis. *Mol. Biol. Cell*, **26**, 2080–2095.
20. van Tran,N., Ernst,F.G.M., Hawley,B.R., Zorbas,C., Ulryck,N., Hackert,P., Bohnsack,K.E., Bohnsack,M.T., Jaffrey,S.R., Graille,M. *et al.* (2019) The human 18S rRNA m6A methyltransferase METTL5 is stabilized by TRMT112. *Nucleic. Acids. Res.*, **47**, 7719–7733.
21. Leismann,J., Spagnuolo,M., Pradhan,M., Wacheul,L., Vu,M.A., Musheev,M., Mier,P., Andrade-Navarro,M.A., Graille,M., Niehrs,C. *et al.* (2020) The 18S ribosomal RNA m(6) A methyltransferase Mettl5 is required for normal walking behavior in Drosophila. *EMBO Rep.*, **21**, e49443.
22. Heurgue-Hamard,V., Graille,M., Scrima,N., Ulryck,N., Champ,S., van Tilbeurgh,H. and Buckingham,R.H. (2006) The zinc finger protein Ynr046w is plurifunctional and a component of the eRF1 methyltransferase in yeast. *J. Biol. Chem.*, **281**, 36140–36148.
23. Liger,D., Mora,L., Lazar,N., Figaro,S., Henri,J., Scrima,N., Buckingham,R.H., van Tilbeurgh,H., Heurgue-Hamard,V. and Graille,M. (2011) Mechanism of activation of methyltransferases involved in translation by the Trm112 'hub' protein. *Nucleic Acids Res.*, **39**, 6249–6259.
24. Fu,D., Brophy,J.A., Chan,C.T., Atmore,K.A., Begley,U., Paules,R.S., Dedon,P.C., Begley,T.J. and Samson,L.D. (2010) Human AlkB homolog ABH8 Is a tRNA methyltransferase required for wobble uridine modification and DNA damage survival. *Mol. Cell. Biol.*, **30**, 2449–2459.
25. Mazauric,M.H., Dirick,L., Purushothaman,S.K., Bjork,G.R. and Lapeyre,B. (2010) Trm112p is a 15-kDa zinc finger protein essential for the activity of two tRNA and one protein methyltransferases in yeast. *J. Biol. Chem.*, **285**, 18505–18515.
26. Songe-Moller,L., van den Born,E., Leihne,V., Vagbo,C.B., Kristoffersen,T., Krokan,H.E., Kirpekar,F., Falnes,P.O. and Klungland,A. (2010) Mammalian ALKBH8 possesses tRNA methyltransferase activity required for the biogenesis of multiple wobble uridine modifications implicated in translational decoding. *Mol. Cell. Biol.*, **30**, 1814–1827.
27. Letoquart,J., Tran,N.V., Caroline,V., Aleksandrov,A., Lazar,N., van Tilbeurgh,H., Liger,D. and Graille,M. (2015) Insights into molecular plasticity in protein complexes from Trm9-Trm112 tRNA modifying enzyme crystal structure. *Nucleic Acids Res.*, **43**, 10989–11002.
28. Fu,Y., Dai,Q., Zhang,W., Ren,J., Pan,T. and He,C. (2010) The AlkB domain of mammalian ABH8 catalyzes hydroxylation of 5-methoxycarbonylmethyluridine at the wobble position of tRNA. *Angew. Chem. Int. Ed. Engl.*, **49**, 8885–8888.
29. van den Born,E., Vagbo,C.B., Songe-Moller,L., Leihne,V., Lien,G.F., Leszczynska,G., Malkiewicz,A., Krokan,H.E., Kirpekar,F., Klungland,A. *et al.* (2011) ALKBH8-mediated formation of a novel diastereomeric pair of wobble nucleosides in mammalian tRNA. *Nat. Commun.*, **2**, 172.
30. Purushothaman,S.K., Bujnicki,J.M., Grosjean,H. and Lapeyre,B. (2005) Trm11p and Trm112p are both required for the formation of 2-methylguanosine at position 10 in yeast tRNA. *Mol. Cell. Biol.*, **25**, 4359–4370.
31. Bourgeois,G., Marcoux,J., Saliou,J.M., Cianferani,S. and Graille,M. (2017) Activation mode of the eukaryotic m2G10 tRNA methyltransferase Trm11 by its partner protein Trm112. *Nucleic Acids Res.*, **45**, 1971–1982.
32. Gu,C., Ramos,J., Begley,U., Dedon,P.C., Fu,D. and Begley,T.J. (2018) Phosphorylation of human TRM9L integrates multiple stress-signaling pathways for tumor growth suppression. *Sci. Adv.*, **4**, eaas9184.
33. Figaro,S., Scrima,N., Buckingham,R.H. and Heurgue-Hamard,V. (2008) HemK2 protein, encoded on human chromosome 21, methylates translation termination factor eRF1. *FEBS Lett.*, **582**, 2352–2356.
34. Ounap,K., Leetsi,L., Matsoo,M. and Kurg,R. (2015) The stability of ribosome biogenesis factor WBSCR22 is regulated by interaction with TRMT112 via ubiquitin-proteasome pathway. *PLoS One*, **10**, e0133841.
35. Leetsi,L., Ounap,K., Abroi,A. and Kurg,R. (2019) The common partner of several methyltransferases TRMT112 regulates the expression of N6AMT1 isoforms in mammalian cells. *Biomolecules*, **9**, 422.
36. van Tran,N., Muller,L., Ross,R.L., Lestini,R., Letoquart,J., Ulryck,N., Limbach,P.A., de Crecy-Lagard,V., Cianferani,S. and Graille,M. (2018) Evolutionary insights into Trm112-methyltransferase holoenzymes involved in translation between archaea and eukaryotes. *Nucleic. Acids. Res.*, **46**, 8483–8499.
37. Armengaud,J., Urbonavicius,J., Fernandez,B., Chaussinand,G., Bujnicki,J.M. and Grosjean,H. (2004) N2-methylation of guanosine at position 10 in tRNA is catalyzed by a THUMP domain-containing, S-adenosylmethionine-dependent methyltransferase, conserved in Archaea and Eukaryota. *J. Biol. Chem.*, **279**, 37142–37152.
38. Hirata,A., Nishiyama,S., Tamura,T., Yamauchi,A. and Hori,H. (2016) Structural and functional analyses of the archaeal tRNA m2G/m22G10 methyltransferase aTrm11 provide mechanistic insights into site specificity of a tRNA methyltransferase that contains common RNA-binding modules. *Nucleic Acids Res.*, **44**, 6377–6390.
39. Urbonavicius,J., Armengaud,J. and Grosjean,H. (2006) Identity elements required for enzymatic formation of N2,N2-dimethylguanosine from N2-monomethylated derivative and its possible role in avoiding alternative conformations in archaeal tRNA. *J. Mol. Biol.*, **357**, 387–399.
40. Gupta,R. (1984) Halobacterium volcanii tRNAs. identification of 41 tRNAs covering all amino acids, and the sequences of 33 class I tRNAs. *J. Biol. Chem.*, **259**, 9461–9471.
41. Gabant,G., Auxilien,S., Tuszynska,I., Locard,M., Gajda,M.J., Chaussinand,G., Fernandez,B., Dedieu,A., Grosjean,H.,

Golinelli-Pimpaneau,B. *et al.* (2006) THUMP from archaeal tRNA:m22G10 methyltransferase, a genuine autonomously folding domain. *Nucleic Acids Res.*, **34**, 2483–2494.
42. Neumann,P., Lakomek,K., Naumann,P.T., Erwin,W.M., Lauhon,C.T. and Ficner,R. (2014) Crystal structure of a 4-thiouridine synthetase-RNA complex reveals specificity of tRNA U8 modification. *Nucleic Acids Res.*, **42**, 6673–6685.
43. Hartman,H., Favaretto,P. and Smith,T.F. (2006) The archaeal origins of the eukaryotic translational system. *Archaea*, **2**, 1–9.
44. Hirata,A., Suzuki,T., Nagano,T., Fujii,D., Okamoto,M., Sora,M., Lowe,T.M., Kanai,T., Atomi,H., Suzuki,T. *et al.* (2019) Distinct modified nucleosides in tRNA(Trp) from the hyperthermophilic archaeon Thermococcus kodakarensis and requirement of tRNA m(2)G10/m(2) 2G10 methyltransferase (Archaeal Trm11) for survival at high temperatures. *J. Bacteriol.*, **201**, e00448-19.
45. Orita,I., Futatsuishi,R., Adachi,K., Ohira,T., Kaneko,A., Minowa,K., Suzuki,M., Tamura,T., Nakamura,S., Imanaka,T. *et al.* (2019) Random mutagenesis of a hyperthermophilic archaeon identified tRNA modifications associated with cellular hyperthermotolerance. *Nucleic Acids Res.*, **47**, 1964–1976.
46. Zheng,L., Baumann,U. and Reymond,J.-L. (2004) An efficient one-step site-directed and site-saturation mutagenesis protocol. *Nucleic Acids Res.*, **32**, e115.
47. Meinnel,T., Mechulam,Y., Fayat,G. and Blanquet,S. (1992) Involvement of the size and sequence of the anticodon loop in tRNA recognition by mammalian and E. coli methionyl-tRNA synthetases. *Nucleic Acids Res.*, **20**, 4741–4746.
48. Mechulam,Y., Guillon,L., Yatime,L., Blanquet,S. and Schmitt,E. (2007) Protection-based assays to measure aminoacyl-tRNA binding to translation initiation factors. *Methods Enzymol.*, **430**, 265–281.
49. Cao,W. and De La Cruz,E.M. (2013) Quantitative full time course analysis of nonlinear enzyme cycling kinetics. *Sci. Rep.*, **3**, 2658.
50. Su,D., Chan,C.T., Gu,C., Lim,K.S., Chionh,Y.H., McBee,M.E., Russell,B.S., Babu,I.R., Begley,T.J. and Dedon,P.C. (2014) Quantitative analysis of ribonucleoside modifications in tRNA by HPLC-coupled mass spectrometry. *Nat. Protoc.*, **9**, 828–841.
51. Kabsch,W. (1993) Automatic processing of rotation diffraction data from crystals of initially unknown symmetry and cell constants. *J. Appl. Cryst.*, **26**, 795–800.
52. Schneider,T.R. and Sheldrick,G.M. (2002) Substructure solution with SHELXD. *Acta Crystallogr. D. Biol. Crystallogr.*, **58**, 1772–1779.
53. Bricogne,G., Vonrhein,C., Flensburg,C., Schiltz,M. and Paciorek,W. (2003) Generation, representation and flow of phase information in structure determination: recent developments in and around SHARP 2.0. *Acta Crystallogr. D. Biol. Crystallogr.*, **59**, 2023–2030.
54. Terwilliger,T. (2004) SOLVE and RESOLVE: automated structure solution, density modification and model building. *J. Synchrotron Radiat.*, **11**, 49–52.
55. Emsley,P. and Cowtan,K. (2004) Coot: model-building tools for molecular graphics. *Acta Crystallogr. D. Biol. Crystallogr.*, **60**, 2126–2132.
56. McCoy,A.J., Grosse-Kunstleve,R.W., Adams,P.D., Winn,M.D., Storoni,L.C. and Read,R.J. (2007) Phaser crystallographic software. *J. Appl. Crystallogr.*, **40**, 658–674.
57. Bricogne,G., Blanc,E., Brandl,M., Flensburg,C., Keller,P., Paciorek,W., Roversi,P., Sharff,A., Smart,O.S., Vonrhein,C. *et al.* (2016) In: *BUSTER version 2.10.2.*, Global Phasing Ltd., Cambridge.
58. Menezes,S., Gaston,K.W., Krivos,K.L., Apolinario,E.E., Reich,N.O., Sowers,K.R., Limbach,P.A. and Perona,J.J. (2011) Formation of m2G6 in Methanocaldococcus jannaschii tRNA catalyzed by the novel methyltransferase Trm14. *Nucleic Acids Res.*, **39**, 7641–7655.
59. Fislage,M., Roovers,M., Tuszynska,I., Bujnicki,J.M., Droogmans,L. and Versees,W. (2012) Crystal structures of the tRNA:m2G6 methyltransferase Trm14/TrmN from two domains of life. *Nucleic Acids Res.*, **40**, 5149–5161.
60. Roovers,M., Oudjama,Y., Fislage,M., Bujnicki,J.M., Versees,W. and Droogmans,L. (2012) The open reading frame TTC1157 of Thermus thermophilus HB27 encodes the methyltransferase forming N(2)-methylguanosine at position 6 in tRNA. *RNA*, **18**, 815–824.
61. Aravind,L. and Koonin,E.V. (2001) THUMP–a predicted RNA-binding domain shared by 4-thiouridine, pseudouridine synthases and RNA methylases. *Trends Biochem. Sci.*, **26**, 215–217.
62. Bujnicki,J.M. (2000) Phylogenomic analysis of 16S rRNA:(guanine-N2) methyltransferases suggests new family members and reveals highly conserved motifs and a domain structure similar to other nucleic acid amino-methyltransferases. *FASEB J.*, **14**, 2365–2368.
63. Bujnicki,J.M. and Radlinska,M. (1999) Is the HemK family of putative S-adenosylmethionine-dependent methyltransferases a 'missing' zeta subfamily of adenine methyltransferases? A hypothesis. *IUBMB Life*, **48**, 247–249.
64. Nakahigashi,K., Kubo,N., Narita,S., Shimaoka,T., Goto,S., Oshima,T., Mori,H., Maeda,M., Wada,C. and Inokuchi,H. (2002) HemK, a class of protein methyl transferase with similarity to DNA methyl transferases, methylates polypeptide chain release factors, and hemK knockout induces defects in translational termination. *Proc. Natl. Acad. Sci. U.S.A.*, **99**, 1473–1478.
65. Li,W., Shi,Y., Zhang,T., Ye,J. and Ding,J. (2019) Structural insight into human N6amt1-Trm112 complex functioning as a protein methyltransferase. *Cell Discov.*, **5**, 51.
66. Metzger,E., Wang,S., Urban,S., Willmann,D., Schmidt,A., Offermann,A., Allen,A., Sum,M., Obier,N., Cottard,F. *et al.* (2019) KMT9 monomethylates histone H4 lysine 12 and controls proliferation of prostate cancer cells. *Nat. Struct. Mol. Biol.*, **26**, 361–371.
67. Machnicka,M.A., Olchowik,A., Grosjean,H. and Bujnicki,J.M. (2014) Distribution and frequencies of post-transcriptional modifications in tRNAs. *RNA Biol.*, **11**, 1619–1629.
68. Gupta,R. (1986) Transfer RNAs of Halobacterium volcanii: sequences of five leucine and three serine tRNAs. *Syst. Appl. Microbiol.*, **7**, 102–105.
69. Demirci,H., Gregory,S.T., Dahlberg,A.E. and Jogl,G. (2008) Crystal structure of the Thermus thermophilus 16 S rRNA methyltransferase RsmC in complex with cofactor and substrate guanosine. *J. Biol. Chem.*, **283**, 26548–26556.
70. Monecke,T., Dickmanns,A. and Ficner,R. (2009) Structural basis for m7G-cap hypermethylation of small nuclear, small nucleolar and telomerase RNA by the dimethyltransferase TGS1. *Nucleic Acids Res.*, **37**, 3865–3877.
71. Tscherne,J.S., Nurse,K., Popienick,P. and Ofengand,J. (1999) Purification, cloning, and characterization of the 16 S RNA m2G1207 methyltransferase from Escherichia coli. *J. Biol. Chem.*, **274**, 924–929.
72. Barraud,P., Gato,A., Heiss,M., Catala,M., Kellner,S. and Tisne,C. (2019) Time-resolved NMR monitoring of tRNA maturation. *Nat. Commun.*, **10**, 3373.
73. McLuckey,S.A., Van Berkel,G.J. and Glish,G.L. (1992) Tandem mass spectrometry of small, multiply charged oligonucleotides. *J. Am. Soc. Mass Spectrom.*, **3**, 60–70.
74. The PyMOL Molecular Graphics System., Version 1.2r3pre Ed., Schrödinger, LLC.
75. Ashkenazy,H., Erez,E., Martz,E., Pupko,T. and Ben-Tal,N. (2010) ConSurf 2010: calculating evolutionary conservation in sequence and structure of proteins and nucleic acids. *Nucleic. Acids. Res.*, **38**, W529–W533.
76. Pettersen,E.F., Goddard,T.D., Huang,C.C., Couch,G.S., Greenblatt,D.M., Meng,E.C. and Ferrin,T.E. (2004) UCSF chimera–a visualization system for exploratory research and analysis. *J. Comput. Chem.*, **25**, 1605–1612.